Global Climate Variations Connected with Sea Surface Temperature Anomalies in the Eastern Equatorial Pacific Ocean for the 1958–73 Period

YI HONG PAN

Institute for Atmospheric Physics, Academia Sinica, Beijing, China

ABRAHAM H. OORT

Geophysical Fluid Dynamics Laboratory/NOAA, Princeton University, Princeton, NJ 08540

(Manuscript received 13 September 1982, in final form 10 March 1983)

ABSTRACT

The sea surface temperature anomalies in the eastern equatorial Pacific Ocean are shown to demarcate a "key region" near 130°W for observed variations in the global general circulation. Various techniques are used to describe global conditions during warm and cold sea surface conditions in the key region based on a global 15-year set of surface and upper air analyses.

Earlier work is confirmed that during warm episodes 1) the westerly jets in both hemispheres are strengthened, and 2) some of the semi-permanent circulation features, such as the intertropical convergence zone, the subtropical high over the western and central Pacific, and the Aleutian low, increase in strength, and *vice versa* for cold episodes.

The time series of monthly-mean atmospheric temperature averaged over the entire mass of the Northern Hemisphere is found to be highly correlated with the sea surface temperature anomalies in the key region. The highest correlation of $r = 0.65$ is found when the atmosphere lags the ocean by 6 months. The maximum temperature response seems to occur in the upper troposphere in the tropics probably associated with variations in convective activity.

1. Introduction

The solar heat stored in the oceans may well constitute one of the main sources of energy for driving observed year-to-year anomalies in the general circulation of the atmosphere. Especially the tropical oceans may be important since, in a climatological sense, they receive the bulk of the solar energy.

Possible relationships between the tropical oceans and world climate have been investigated for almost a century. Most noteworthy are the studies by Sir Gilbert Walker and E. W. Bliss (1932, 1937), Berlage (1966) and Bjerknes (1969) on the, so-called, Southern Oscillation, Walker oscillation and the El Niño phenomenon. For a discussion of the extensive literature on these phenomena and their interrelationships see Julian and Chervin (1978) and Rasmusson and Carpenter (1982).

The present study was motivated by previous work by one of the authors (e.g., Pan, 1978) relating sea-surface temperature fluctuations in the equatorial Pacific with later fluctuations in important climatic parameters over China, such as the position and intensity of the subtropical high and the frequency of typhoons. Here we will focus on possible relations between anomalies in the *global* atmospheric circulation and tropical surface temperature anomalies, which may provide a key for understanding year-to-year variations in the global climate.

2. Data base

Two global data sets were available to investigate the problem. The first set consisted of surface marine observations taken from ships for the 15-year period, May 1958 through April 1973. All available surface ship data were averaged in 2° latitude by 2° longitude squares for each month of the 15-year period. Only squares with more than three observations during a month were used in the analyses. The distribution of the input data used for the climatological (1964–73) mean January analyses at the ocean surface is displayed in Fig. 1. This figure shows a good data coverage north of about 40°S, but a poor one south of this latitude. The situation in the Southern Hemisphere is even worse during the southern winter, June through August. However, in the tropics, where the main emphasis of our paper is, the distribution seems adequate to show the large-scale features of air–sea exchange. Also our analysis scheme (Oort, 1983) helps to better define the anomaly fields by feeding in information from adjacent areas with better data coverage.

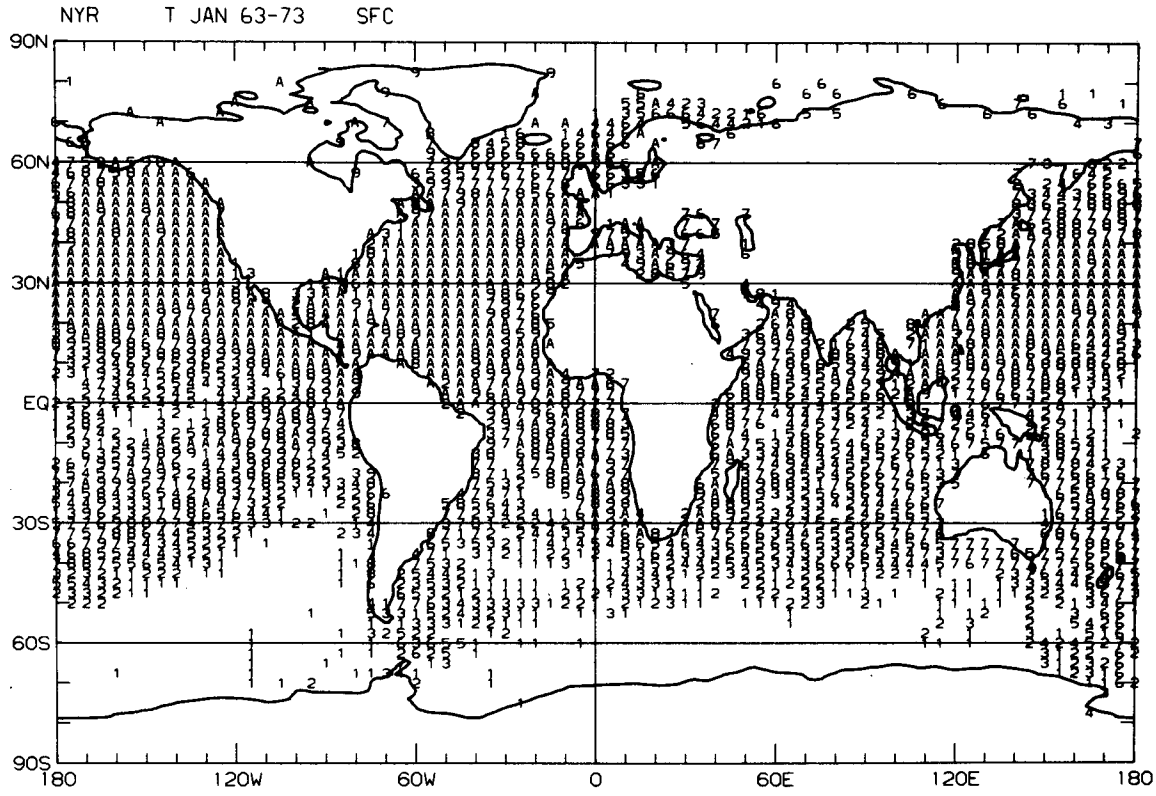

FIG. 1. Distribution of input data used in the surface analyses for the month of January during the 1964–73 period, and number of years of observations available, ranging between 1 and 10 (=A) years. Data over oceans are from 2° × 2° grid averaged surface ship reports (only plotted for every 5° longitude).

The second data set consists of upper air observations from the global rawinsonde network for the same 15-year period. In this case, only stations with 10 or more observations were used in the analyses for a month. The station network is displayed in Fig. 2. Evidently there are large holes in the rawinsonde network over the oceans, especially in the 40°–60°S latitude belt. Therefore, the results in this paper should be considered as tentative over those regions, because the analyses only represent interpolations or extrapolations from data-rich regions.

Since global analyses were attempted for the last 10 years only, much of the present study will deal with results from the 1963–73 period. After careful screening of the data for errors the station data were analyzed objectively onto a latitude-longitude grid using a zonal average of the data in a latitudinal belt as an initial guess. The data reduction, analysis procedures and general reliability of the results are discussed extensively in Oort (1983).

3. Selection of key region

It appears of interest to investigate how sensitive various climate parameters are to anomalies in the surface temperature of the tropical oceans. First of all, the month-to-month variability of the sea surface temperature for the 10-year period, May 1963 through April 1973, is presented in Fig. 3. It shows the standard deviation of monthly-mean sea surface temperatures averaged over the 10°S to 5°N latitude belt as a function of longitude after the normal annual cycle was removed. A 15°-wide latitude belt, centered at 2.5°S, was chosen because it tends to cover the strongest sea surface temperature anomalies which are found on the average somewhat south of the equator (see e.g., Rasmusson and Carpenter, 1982). The curve shows that the strongest variability tends to occur in the eastern equatorial Pacific Ocean, east of the date line (see also Weare *et al.*, 1976). In the other oceans, much weaker relative maxima are observed in the eastern Atlantic and western Indian Oceans.

It is well-known that the westerly currents in the upper troposphere are important indicators of the character of the atmospheric general circulation. Therefore we have computed global maps of the correlation coefficient between anomalies in the sea surface temperature for various locations along the equator and anomalies in the zonal wind at 200 mb (see e.g. Fig. 9a). As a measure of the sensitivity, we counted the number of points on our 2.5° latitude × 5° longitude grid in the tropical belt, 30°S–30°N,

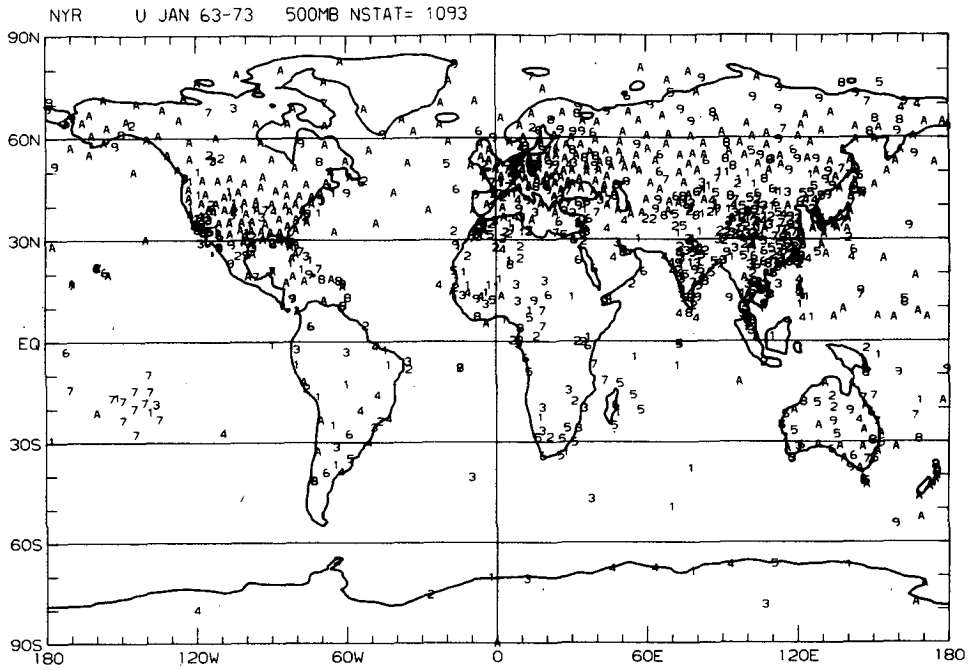

FIG. 2. Distribution of rawinsonde data used in the 500 mb analyses for the months of January during the 1964–73 period, and number of years of observations available, ranging between 1 and 10 (=A) years (total number of stations over globe for January is 1093).

with a value of the correlation coefficient $|r| \geq 0.4$, and divided this number by the total number of grid points in the belt. The choice of a cut off value of $r = 0.4$ is somewhat arbitrary; it indicates, according to Table 1, with 95% confidence that the true $|r|$ has a value between ~0.2 and 0.6. The fractions obtained are displayed in Fig. 4 for the case that the 200 mb wind lags the sea surface anomalies by −1, 0 and +1 month. The highest correlations are found for the eastern equatorial Pacific Ocean, and only negligible correlations for the western Pacific and the Atlantic and Indian Oceans. There are no significant differences between the different lags. This graph, together with the variability curve in Fig. 3, justifies the choice of the area centered at 2.5°S, 130°W as a "key region" for possible connections with the global circulation (see also Pan, 1978, and later discussion of Fig. 14). Both to the east of the key region, near the coast of South America, as well as to the west, near the date line, the correlations drop off sharply.

To test whether the sea surface temperature anomalies in the key region are really unique in affecting the 200 mb tropical winds, we have repeated the same calculations described above for a few selected sea surface points at other latitudes. We found that none of the selected points in the Western Pacific (150°E), eastern Pacific (150°W) or central Atlantic (30°W) for the latitudes 20°S, 20°N, 40°N and 60°N showed an appreciable correlation with the 200 mb zonal wind in the tropics. In fact, the fraction of points in the 30°S–30°N zone with a correlation coefficient $|r| \geq 0.4$ was never more than a few percent. Compared with the value of 26% at lag = 0 in the vicinity of the key region (see Fig. 4), this calculation dem-

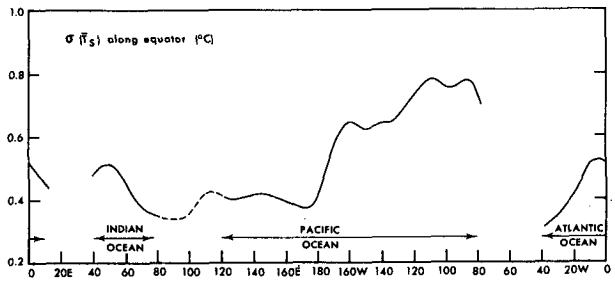

FIG. 3. Standard deviation of the monthly-mean sea surface temperature (°C) as a function of longitude for the 10°S–5°N latitude belt.

TABLE 1. Lower and upper 95% confidence limits for various correlation coefficients for 120 (60) degrees of freedom. [Computed after Spiegel (1961) using Fisher's z-transformation for r.]

r	Lower limit	Upper limit
0.20	0.02 (−0.06)	0.37 (0.43)
0.30	0.13 (0.05)	0.45 (0.51)
0.40	0.24 (0.16)	0.54 (0.59)
0.50	0.35 (0.28)	0.62 (0.67)
0.60	0.47 (0.41)	0.70 (0.74)
0.70	0.60 (0.54)	0.78 (0.81)

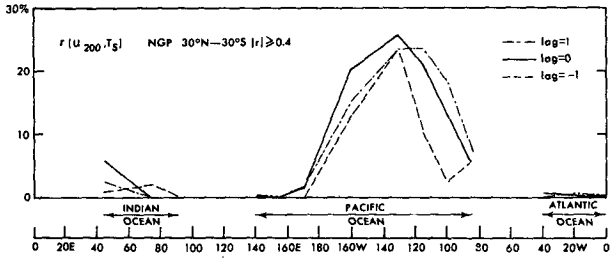

FIG. 4. Percentage of total number of grid points in the tropical belt (30°S–30°N) for which $\bar{u}_{200}$ is strongly correlated ($|r| \geq 0.4$) with the sea surface temperature anomalies at various longitudes in the 10°S–5°N belt. The three curves are for lag = −1 (anomaly in $\bar{u}_{200}$ precedes anomaly $\bar{T}_s$ by 1 month), lag = 0 and lag = +1.

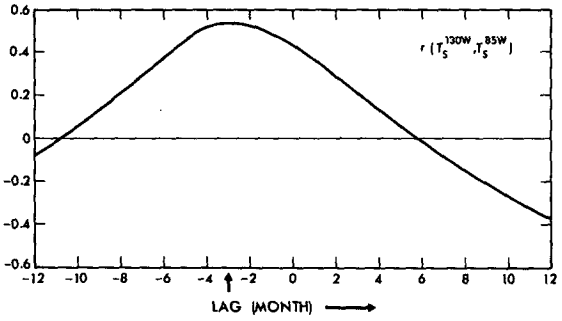

FIG. 6. Correlation coefficient between the (unfiltered) monthly sea surface temperatures at 2.5°S, 130°W and 2.5°S, 85°W for different lags during the 15-year period. (A negative lag means that the 85°W anomalies precede the 130°W anomalies.)

onstrates the apparent uniqueness of the eastern equatorial Pacific Ocean.

A westward propagation of the anomalies in the sea surface temperature along the equator was described extensively by Rasmusson and Carpenter (1982). Our analyses, based on a similar set of ship data but differently analyzed, show a comparable propagation as demonstrated in Figs. 5 and 6 for the May 1958–April 1973 period. Figs. 5a and b show the time series of the monthly-mean anomalies for the key region at 130°W and for a region off the coast of Ecuador at 85°W, respectively, each averaged over four grid points at 10°S, 5°S, equator and 5°N. The normal annual cycles were removed. Further, smoothed lines are added to emphasize longer term variations. In both figures a temperature fluctuation with a time scale of about 40 months is in evidence, indicating alternating warm and cold regimes in the eastern equatorial Pacific Ocean. Visual inspection, as well as the actual calculation of the correlation coefficient at different lags in Fig. 6, show that the anomalies in the key region at 130°W lag the anomalies at 85°W near the coast of Ecuador by about 3 months. Although the variations in sea surface temperature along the coast of Peru and Ecuador are spectacular and of great economic significance, the variations at 130°W seem to be more important for the tropical atmosphere as a whole as was shown earlier in Fig. 4.

The reason for the apparent significance of the equatorial ocean near 130°W longitude seems to lie in the fact that it best represents the average temperature of the entire eastern equatorial Pacific. In fact, according to Fig. 7, the sea temperature anomalies near 130°W show a peak correlation coefficient of $r = 0.9$ at lag = 0 with the average sea surface anomalies in the entire 20°S–20°N, 80°W–180°W area, whereas the anomalies at 85°W show only a maximum correlation of $r = 0.6$ one month before the anomalies in the area mean occur.

To clarify the connections between the temperature anomalies in the key region with those in the rest of the world ocean we have prepared a few correlation maps using all months from the 10 year pe-

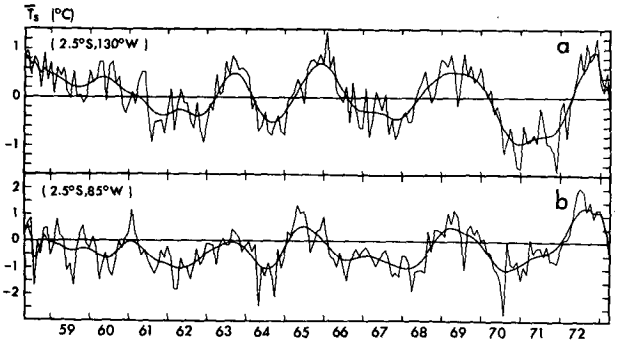

FIG. 5. Time series of the monthly-mean sea surface temperature at the equator for (a) the key region, 130°W, and (b) 85°W during the 15-year period, May 1958 through April 1973. The normal annual cycle was removed in each time series. The markings along the abscissa indicate the January of a particular year. The smoothed lines were obtained by applying a 15-point Gaussian-type filter with weights 0.012, 0.025, 0.040, 0.061, 0.083, 0.101, 0.117 and 0.122 at the central point.

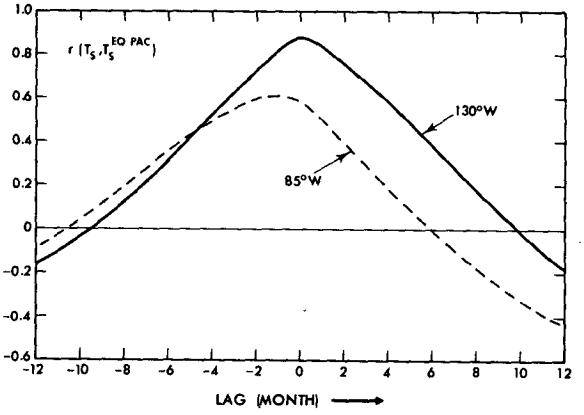

FIG. 7. Correlation coefficients of the 15-year (unfiltered) monthly sea surface temperature series at 2.5°S, 130°W and 2.5°S, 85°W with the area-averaged temperature of the entire eastern equatorial Pacific Ocean (20°S–20°N, 80°–180°W).

riod, May 1963 through April 1973, irrespective of season. Thus Fig. 8 shows global correlation patterns at various lags. At a lag of −3 months (Fig. 8a), the significant anomalies (roughly corresponding to $|r| \geq 0.3$; see discussion of Table 1 below) are limited to the eastern equatorial Pacific, and are centered near 5°S about 20° to the east of the key region. At zero lag (Fig. 8b) the highest correlations have progressed westward and are centered over the key region, as one would expect. Another important difference with the pattern in Fig. 8a is that all tropical oceans, except for a small region in the western Pacific, show the same positive sign, whereas the mid-latitude oceans consistently show a negative sign. At lags of +3 and +6 months (Figs. 8c and 8d), the largest correlations are found to occur to the west of the key region (corresponding to a further westward propagation of the anomalies), and away from the equator. Of interest are the increasingly positive correlations in the tropical Atlantic and Indian Oceans, perhaps pointing to a gradual transmission of the signal (through the atmosphere?) from the Pacific to the other oceans. Thus the tropical oceans, as a whole, seem to remain warm (cold) even 6 months following the maximum (minimum) temperatures in the key region. Our results agree well with the typical El Niño sequence described by Rasmusson and Carpenter (1982) in their peak, transition and mature phase composites for the tropical Pacific.

To give a measure of the reliability of the individual correlation coefficients and of the correlation maps presented in this article we have computed 95% confidence limits for various values of r. Because r is not normally distributed the confidence limits were calculated using Fisher's z-transformation

$$z = \tfrac{1}{2} \ln[(1 + r)/(1 - r)]. \quad (1)$$

The z statistic is approximately normally-distributed with a standard deviation $\sigma_z = (N - 3)^{-1/2}$ where N = number of degrees of freedom (Spiegel, 1961, pp. 247 and 264). Table 1 shows the results for $N = 120$, equivalent with the assumption that all 120 monthly values from the 10-year sample are independent, and also for $N = 60$ where only every other month is assumed to be independent. From inspection of this table it seems reasonable to conclude that values of $|r| \geq 0.3$ are significantly different from zero at the 95% confidence level. However, on the horizontal maps, as shown in Fig. 8, one would expect about 5% of the grid points to have values of $|r| \geq 0.3$ just by

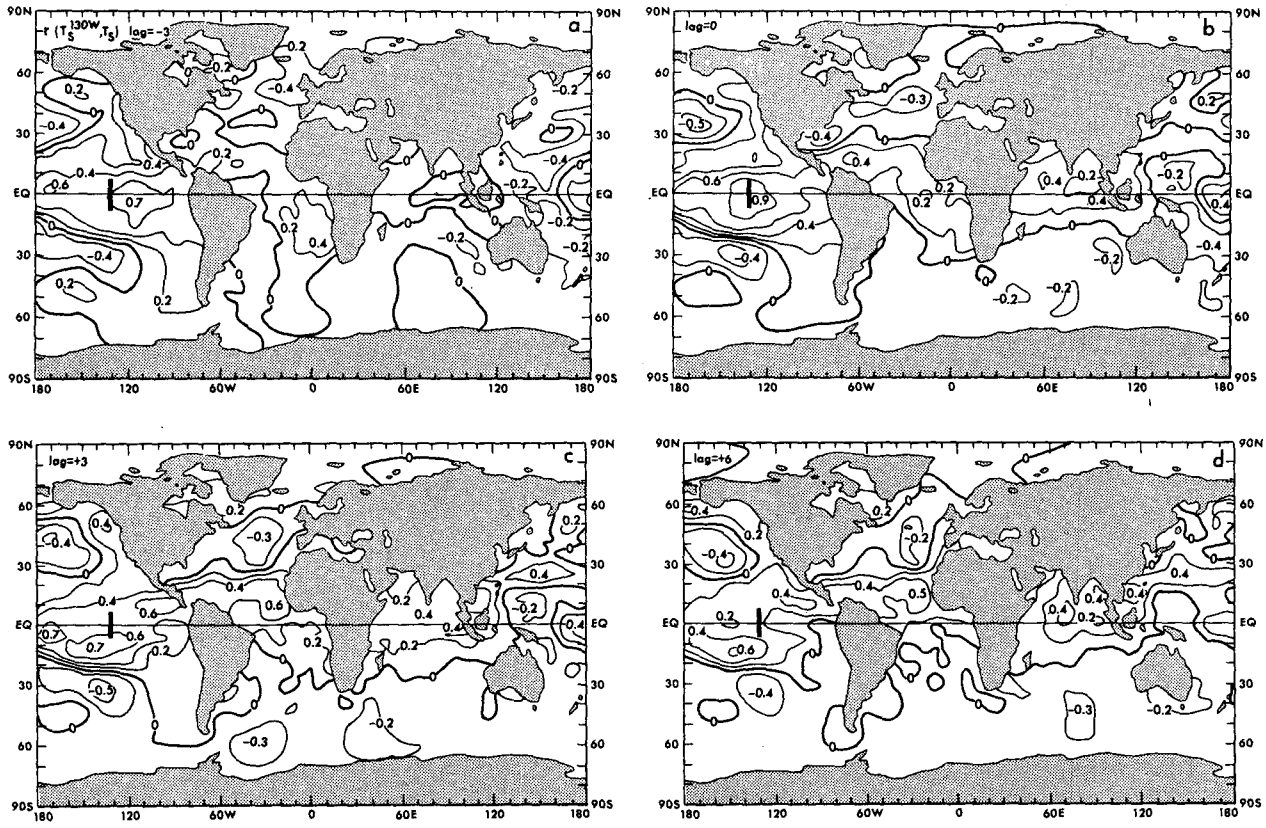

FIG. 8. Maps of the correlation coefficient of the sea surface temperature anomalies in the key region with those in the rest of the oceans for various lags (in months); a positive lag indicates that the anomaly follows the one in the key region. Numbers not attached to isolines indicate extreme values. Extensive areas with $|r| \geq 0.3$ are statistically significant at the ≥95% level.

chance, and perhaps even a greater percentage considering that the samples at the various grid points are not independent of each other. These points should be kept in mind when considering the various correlation maps. For more thorough tests of the significance level see Chen (1982).

4. Correlations with atmospheric winds

The nature of possible large-scale interactions between the sea surface temperature in the key region at 2.5°S, 130°W and global wind patterns is depicted through maps of correlation coefficients for the May 1963 through April 1973 period in Figs. 9a through 9e. Chosen are those parameters that best characterize the overall circulation in the atmosphere. Thus we selected in Figs. 9a, b the monthly-mean zonal and meridional wind components at 200 mb in the upper troposphere where the jet streams are found, in Fig. 9c the vertical velocity field $\bar{\omega}$ at 500 mb in the mid-troposphere, and, finally, in Figs. 9d and 9e the monthly-mean zonal and meridional wind component just above the ocean surface. In the regions where $|r| > 0.3$ the correlation is significantly different from zero at the 95% or greater confidence level (see discussion in previous section).

The computed correlation fields can be interpreted more easily if we first describe the schematic picture envisioned by Bjerknes (1969) for the circulation anomalies associated with exceptionally warm sea surface temperatures in the eastern equatorial Pacific Ocean. During warm episodes, Bjerknes argues, the normal east–west Walker circulation with intense rising motion in the vicinity of Indonesia and sinking over the eastern tropical Pacific weakens, whereas the local Hadley circulation with rising air near the equator and sinking air in the subtropics intensifies over the eastern Pacific. The increased Hadley cell leads then, through conservation of absolute angular momentum, to stronger westerly winds in the subtropical jets.

Returning to our figures, the correlation maps support and further expand Bjerknes hypotheses. For example, Fig. 9c shows that relatively warm sea temperatures in the key region are associated with anomalous rising motion over the central and most of the eastern equatorial Pacific and with sinking motion over both the western Pacific, the eastern Pacific east of 120°W, and the subtropics of both hemispheres, whereas cold sea surface temperatures are associated with the reverse anomalous vertical motions. These vertical motion patterns correspond well with the long-wave radiation anomaly maps obtained recently by Lau and Chan (1983). Because of the close association between long-wave radiation flux and precipitation in the Tropics their maps indicate a relative increase in precipitation over our areas of rising motion and a decrease over the areas of sinking motion. At the same time the 200 mb subtropical westerlies near 25°N and 25°S in Fig. 9a strengthen during the warm regime, while an abnormal westward wind occurs at 200 mb over the equatorial Pacific. Figs. 9a through 9e together suggest that during warm episodes a local north–south Hadley circulation intensifies over the eastern and central Pacific Ocean (stronger equatorward winds at the surface of both hemispheres in Fig. 9e and stronger poleward winds at 200 mb in Fig. 9b with rising motion over the equator in Fig. 9c) at the cost of the east–west Walker circulation (surface westerlies over the equator in Fig. 9d and upper-air easterlies in Fig. 9a). Of course, during cold episodes the picture should be reversed. We should mention here the weak, but systematic circulation anomalies to the east of the key region, that resemble the anomalies over Indonesia rather than those over the central and eastern Pacific Ocean west of 120°W. In fact, there is an indication of sinking motion near 100°W, limiting the longitudinal extent of the rising branch of the reverse Walker-Oscillation to the 150°E–120°W sector. Shukla and Wallace (1983) found a similar vertical motion pattern along the equator in their numerical simulation experiments. We may add that many other important characteristics of El Niño–Southern Oscillation phenomena have been simulated to some extent in numerical experiments (see e.g., Rowntree, 1972, and Keshavamurty, 1982).

Considering now the tropical Atlantic and Indian Oceans, we find the same general tendency for a strengthening (weakening) of the meridional Hadley circulation and of the subtropical zonal jet streams around the globe during warm (cold) sea surface temperatures at 2.5°S, 130°W. However, the effects are less well-defined than over the Pacific Ocean.

Away from the tropics the signals are weaker, but some features such as the tendency for more westward flow near 60°N probably connected with a stronger Ferrel circulation during warm episodes seem significant.

Earlier studies of the tropical wind field at 200 mb by Chiu and Lo (1979) and Arkin (1982) and at the surface by Pazan and Meyers (1982) show the same type of wind variations as those depicted in Fig. 9.

As a more intuitive test of the significance of the points on the correlation maps we have prepared Fig. 10. In this figure, the actual time series of $\bar{u}$ and $\bar{v}$ at 200 mb are plotted for some selected points with relatively high values of the correlation coefficient. Although the correlation maps were only based on the last 10 years of record, we show here the total 15-year record. In addition to the plots of actual values smoothed curves were drawn to enhance the long-term variations. Further, for easy reference, the smoothed sea-surface temperature curve for the key region from Fig. 5a is added as a dashed line. The computed values of the correlation coefficients with

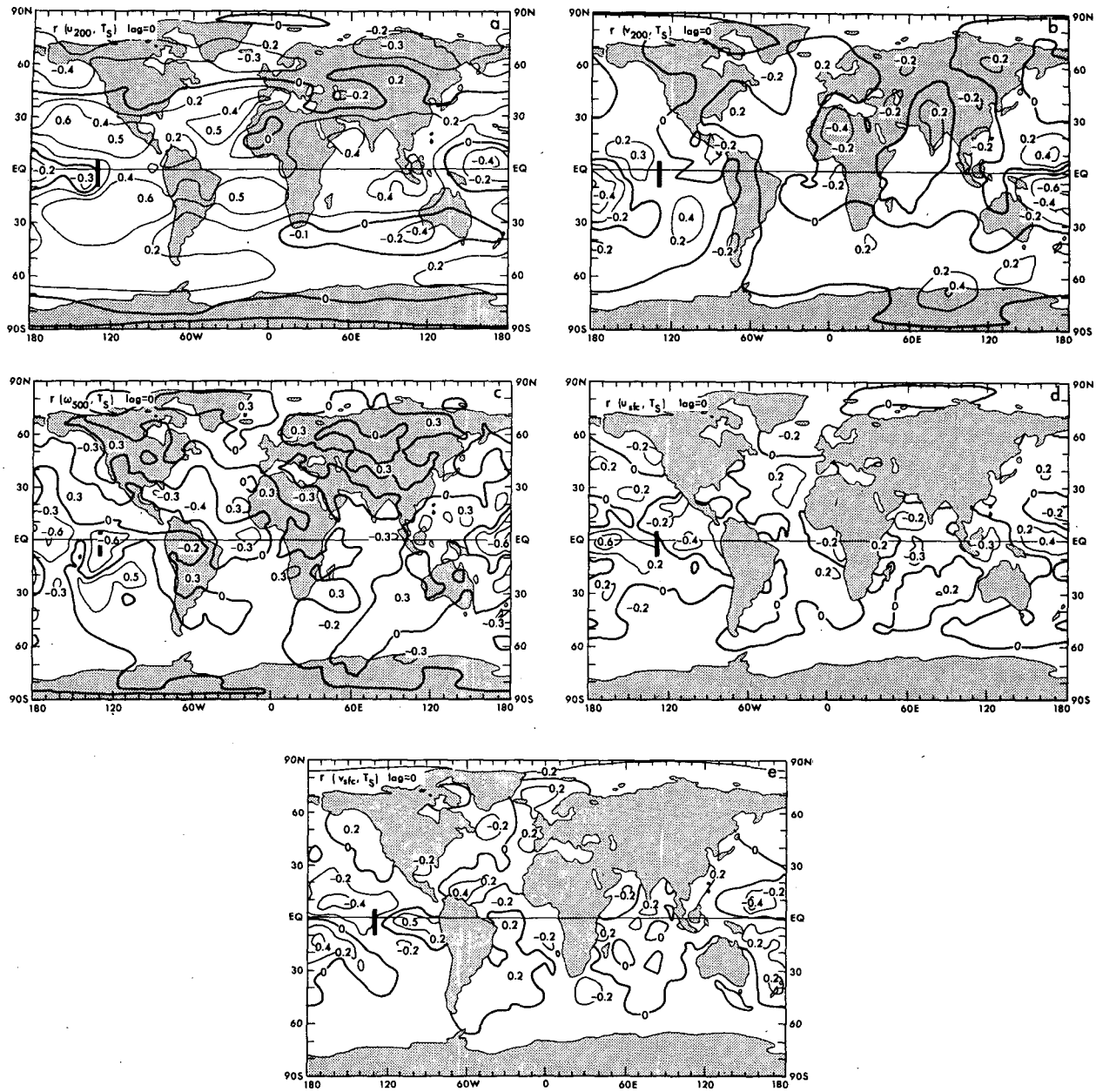

FIG. 9. Maps of the correlation coefficient of the sea surface temperature anomalies in the key region with the (a) eastward wind component at 200 mb, $\bar{u}_{200}$, at lag = 0 for the May 1963–April 1973 period. Numbers not attached to isolines indicate extreme values. Extensive areas with $|r| \geq 0.3$ are statistically significant at the ≥95% level; (b) for the northward wind component at 200 mb, $\bar{v}_{200}$; (c) for vertical "pressure" (positive if directed downward) velocity at 500 mb, $\bar{\omega}_{500}$; (d) for the eastward wind component at the surface, $\bar{u}_{\text{sfc}}$; and (e) for the northward wind component at the surface, $\bar{v}_{\text{sfc}}$.

the (unsmoothed) T_s curve are tabulated in Table 2 for various lags. A careful inspection of the graphs confirms our earlier conclusion that a correlation coefficient larger than ~0.3 or smaller than −0.3 would be physically significant and real. In general, similar plots for the grid points where $|r| < 0.3$ (not presented here) do not show a clear resemblance with the T_s curve in the key region. Although this approach does not pretend to give an exact measure of the significance, it is another indication that a cutoff criterion of $|r| = 0.3$ represents a realistic estimate. As shown in Table 2, the highest correlations are found near lag = 0.

5. Comparisons between warm and cold episodes

A more quantitative idea of the differences in the state of the atmosphere when the sea surface tem-

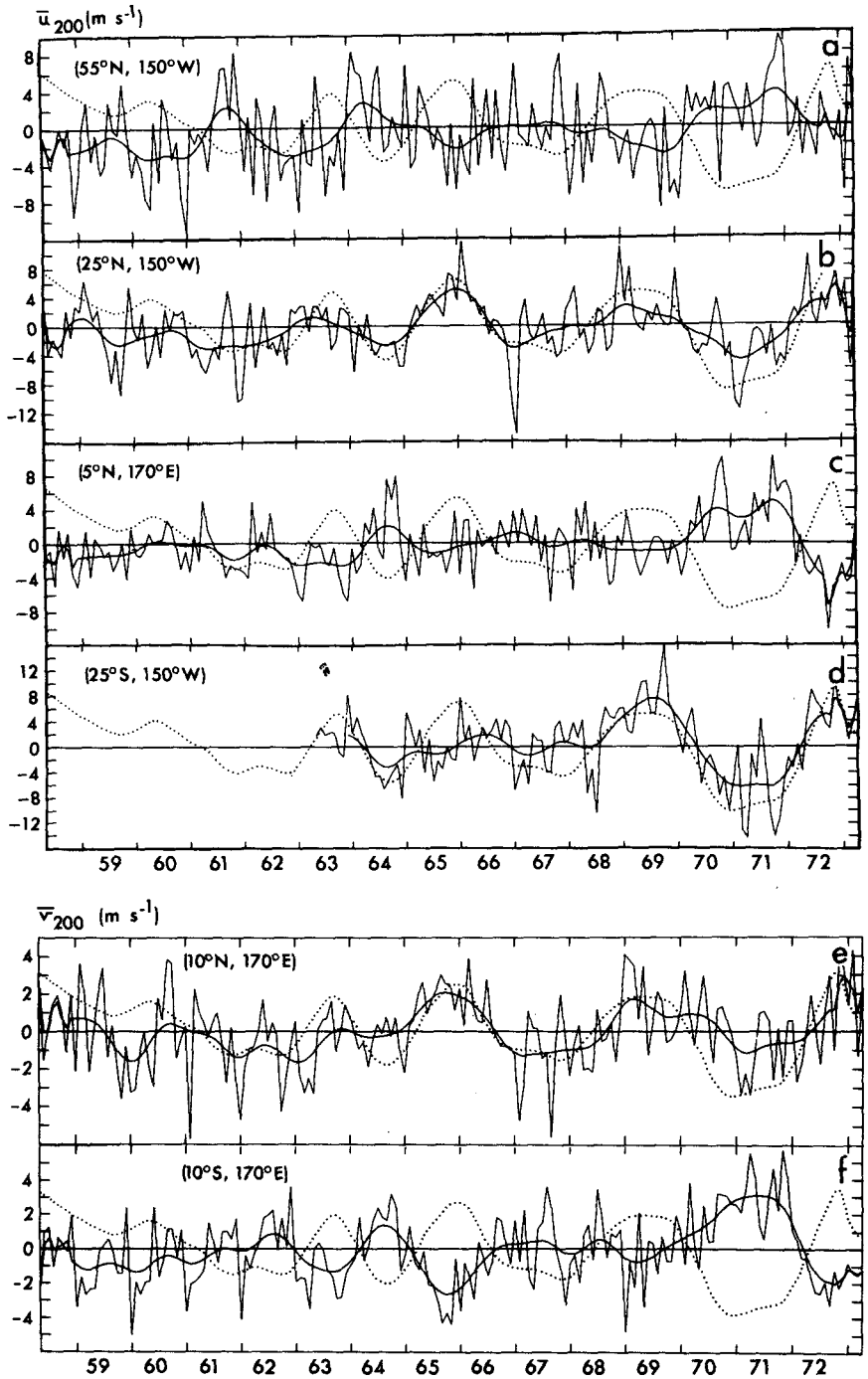

FIG. 10. Time series of monthly-mean anomalies (m s^{-1}) in $\bar{u}_{200}$ for May 1958 through April 1973 at (a) 55°N, 150°W, (b) 25°N, 150°W, (c) 5°N, 170°E, (d) 25°S, 150°W, and of the monthly-mean anomalies (m s^{-1}) in $\bar{v}_{200}$ at (e) 10°N, 170°E and (f) 10°S, 170°E. For easy comparison a dashed curve is added which represents the temperature record in the key region (also see legend Fig. 5).

peratures in the eastern equatorial Pacific Ocean are relatively warm and when they are cold, is gained from an inspection of Figs. 11b through 11d. These maps show global distributions of the averaged difference between five warm December–February cases (1963/64, 1965/66, 1968/69, 1969/70 and 1972/73) and five cold ones (1964/65, 1966/67, 1967/68, 1970/71 and 1971/72). The criterion used to decide whether

TABLE 2. Correlation coefficient between sea surface temperature anomalies in the key region (2.5°S, 130°W) and wind speed anomalies for various locations at 200 mb during the 15-year period, May 1958 through April 1973.

		Lag (month)						
		−6	−4	−2	0	2	4	6
$\bar{u}_{200}$	60°N, 20°W	−0.17	−0.16	−0.17	−0.19	−0.20	−0.15	−0.09
	55°N, 150°W	−0.11	−0.24	−0.28	−0.34	−0.27	−0.15	−0.11
	25°N, 150°W	0.27	0.34	0.41	0.40	0.32	0.25	0.13
	5°N, 170°E	−0.23	−0.34	−0.39	−0.34	−0.32	−0.26	−0.14
$\bar{v}_{200}$	10°N, 170°E	0.06	0.07	0.23	0.36	0.36	0.30	0.21
	10°S, 170°E	−0.33	−0.46	−0.57	−0.51	−0.35	−0.28	−0.20

a December–February (DJF) season would be included as a warm or as a cold case, was based on the T_s-anomaly curve for the key region in Fig. 5a.

In Fig. 11 areas of significant difference at the 95% level (or greater) are shaded. In order to estimate the level of significance the t-statistic was computed at each grid point (Panofsky and Brier, 1958, p. 63):

$$t = (\bar{x}_1 - \bar{x}_2)[(s_1^2 + s_2^2)/(n-1)]^{-1/2}, \quad (2)$$

In this expression, n is the number of warm (or cold) cases, $\bar{x}_1$ and s_1^2 the sample mean and variance of the parameter x for the warm cases, and $\bar{x}_2$ and s_2^2 the corresponding sample mean and variance for the cold cases. By comparing the computed t-values with the entries in a standard Student's t table using the appropriate number of degrees of freedom $N = 2n - 2$, one can determine the desired level of significance. In the DJF case, shown in Fig. 11, those areas

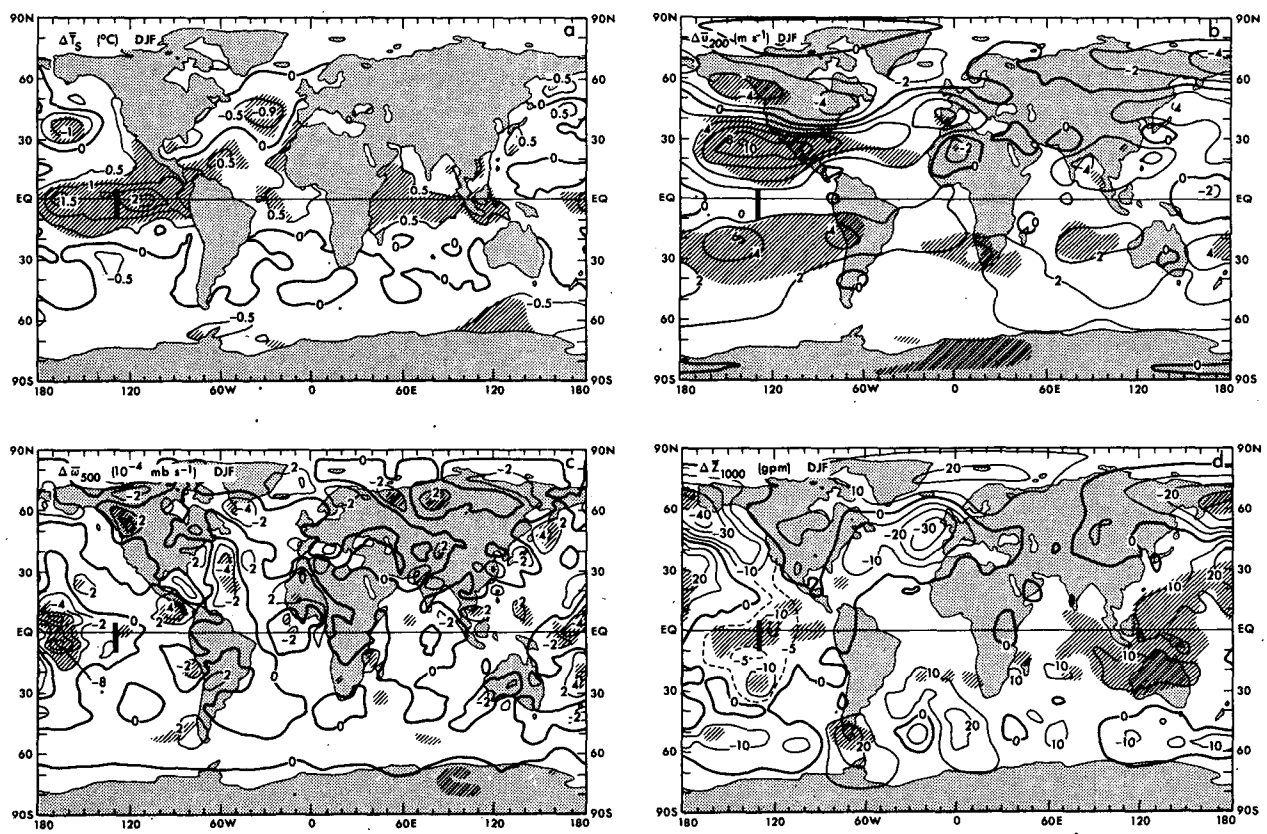

FIG. 11. Map of (a) the average sea-surface temperature difference (°C) between the December–February seasons that $\bar{T}_s$ in the key region was relatively warm and the seasons that it was relatively cold. Numbers not attached to isolines indicate extreme values. The areas with significant ΔT_s at the ≥95% level are shaded; (b) map of $\bar{u}_{200}$ (m s^{-1}). Note that positive values indicate relative eastward flow or westerlies; (c) map of $\bar{\omega}_{500}$ (10^{-4} mb s^{-1}). Note that negative values indicate relative rising motions; and (d) map of the height of the 1000 mb pressure surface, $\bar{z}_{1000}$ (gpm).

are shaded where $|t| \geq 2.3$, indicating a significance of 95% or greater for our sample of five northern winters ($N = 8$). In the June–August (JJA) case to be discussed later in connection with Fig. 12 the shaded areas indicate where $|t| \geq 2.8$, which is the appropriate value of 95% significance for the sample of three northern summers ($N = 4$).

First of all, Fig. 11a shows the "warm–cold" sea surface temperature map. As expected, the largest differences are found in the eastern equatorial Pacific with a peak value greater than 2°C just east of the key region. This map resembles our earlier Fig. 8b as well as the composite maps for the tropical Pacific computed by Rasmusson and Carpenter (1982) for, what they call, the transition and mature phases of a typical El Niño year (see their Figs. 20a and 21a). Our map shows, as it should, somewhat larger values because it represents the difference between El Niño and non-El Niño years rather than the deviation from normal as in Rasmusson and Carpenter's case. Interestingly, the equatorial Atlantic and Indian Oceans are also warmer, by about 0.5°C. On the other hand, in middle and high latitudes the oceans tend to be cooler except in the western Pacific. Nevertheless, we find that the sea surface temperature averaged over all Northern Hemisphere oceans varies similarly as the temperature in the key region with $r_{max} = 0.5$ at a lag of about 3 months.

The instantaneous atmospheric "response" in Fig. 11b indicates a significant increase in the eastward subtropical jets of both hemispheres of up to 10 m s^{-1} near 30°N, 140°W, and increases in westward winds (not significant at 95% level) in middle and high latitudes of the Northern Hemisphere. The increase in westward winds over the equatorial Pacific between 170°W and 140°E is not significant at the 95 percent level but was found to be significant in the 120-month sample shown in Fig. 9a. All these features agree well with similar analyses by van Loon and Rogers (1981; see their Figs. 5 and 7) and Arkin (1982), as well as with our correlation map in Fig. 9a which was based on all 120 monthly analyses. Similarly, the vertical velocity map at 500 mb in Fig. 11c agrees with the corresponding correlation map in Fig. 9c. Strongest relative rising motions of -8×10^{-4} mb s^{-1}, or about 12 mm s^{-1}, are found just west of the key region. Finally, a map of the change in height of the 1000 mb pressure level (extrapolated, where necessary, into the mountains) which is practically equivalent with a map of the change in surface pressure (1 mb $\approx$ 8 gpm), is shown in Fig. 11d. The relatively low pressures in the eastern part of the South Pacific Ocean and the high pressures over the western part as well as over most of the South Atlantic and Indian Oceans are similar to the correlation maps for the Southern Oscillation presented by Berlage (1966, see his Fig. 4). These patterns indicate that important east–west shifts of mass occur associated with El Niño. As noted previously by other authors, there must be a close connection between the Southern Oscillation and the El Niño phenomenon. Other interesting features in Fig. 11d are a pressure rise over the subtropical high in the western and central North Pacific and pressure falls in the vicinity of the semipermanent Aleutian low. These results agree well with those from Namias (1976), Trenberth and Paolino (1981), and van Loon and Madden (1981, see their Fig. 5). Because of the large day-to-day variability over midlatitudes in the Atlantic Ocean, the strong pressure drops west of Europe are not significant.

We have added some maps for the northern summer season, June through August, in Figs. 12a and 12b. Because only three warm (1963, 1968, 1972) and three cold (1964, 1970, 1971) JJA cases could be defined, the maps are generally less reliable than those for the northern winter as demonstrated by the smaller shaded areas. Nevertheless, the summer temperature map resembles the winter map in Fig. 11a with the largest differences in the equatorial eastern Pacific. The secondary maximum in the eastern equatorial Atlantic suggests perhaps a somewhat similar

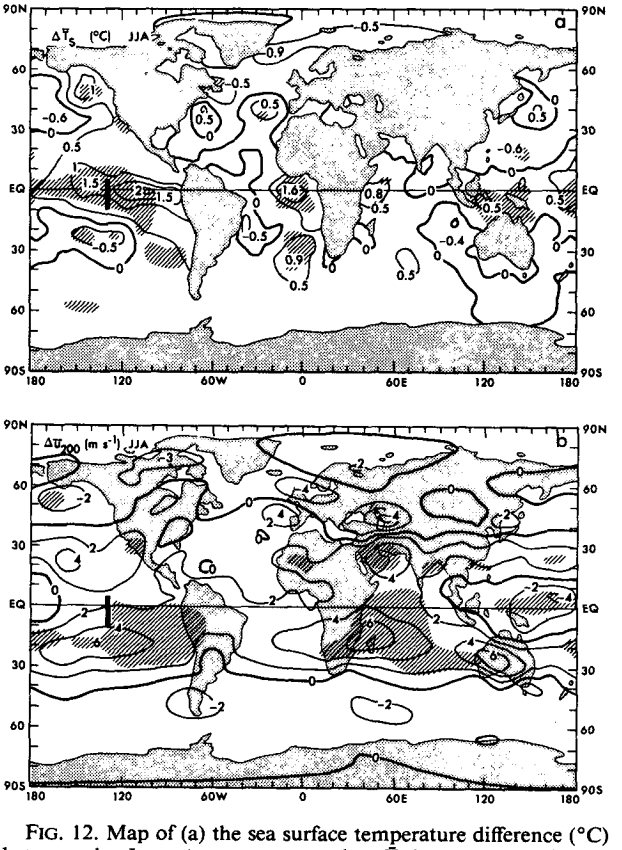

FIG. 12. Map of (a) the sea surface temperature difference (°C) between the June–August seasons that $\bar{T}_s$ in the key region at 130°W was relatively warm and the seasons that it was relatively cold. Numbers not attached to isolines indicate extreme values. The areas with significant ΔT_s at the ≥95 percent level are shaded. (b) Map of $\bar{u}_{200}$ (m s^{-1}).

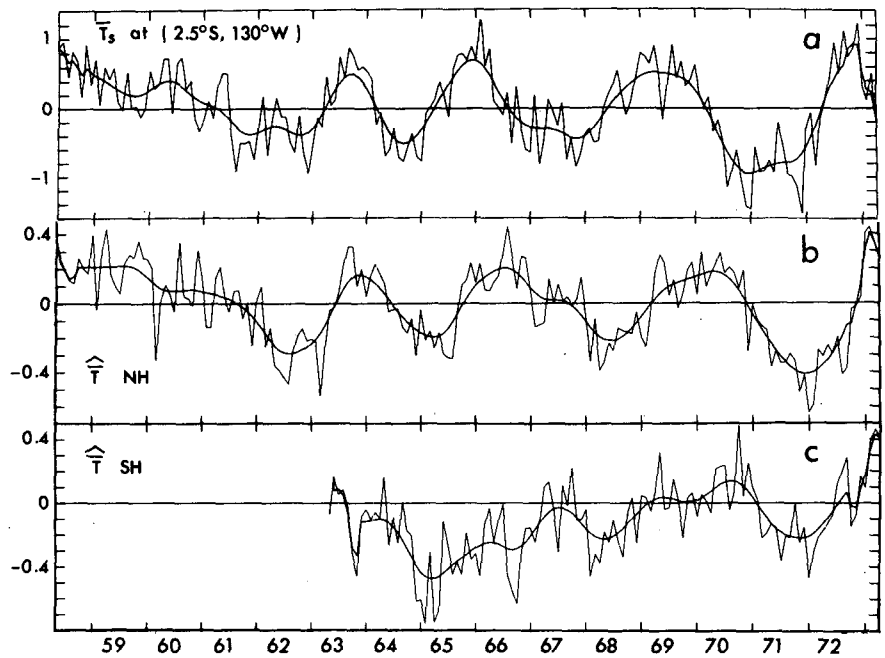

FIG. 13. Time series of (a) the monthly-mean sea surface temperature (°C) in the key region (2.5°S, 130°W) and the air temperature (°C) averaged vertically and horizontally over the entire mass of (b) the Northern and (c) the Southern Hemisphere for the period, May 1958 through April 1973. The 1963–73 mean annual cycle has been removed (see also legend Fig. 5).

behaviour in the Atlantic and Pacific Oceans. The atmospheric "response" in the zonal wind at 200 mb in Fig. 12b also resembles the DJF map in Fig. 11b, but with some important differences. First, the main increase in westerlies appears to occur in the Southern rather than in the Northern Hemisphere. A related factor may be that, when the key region becomes warmer, mainly the Hadley cell of the winter hemisphere intensifies, while the summer-hemisphere Hadley cell is less affected (see later discussion of Fig. 17). A second difference with the northern winter case is the pronounced increase in easterlies over the western and central equatorial Pacific showing more clearly the weakening of the east–west Walker oscillation. These seasonal differences in the atmospheric response could be associated with normal seasonal differences in the mean wind structure affecting the transfer of anomalies across tropical latitudes.

6. Correlations with atmospheric temperature

So far we have not considered the temperature variations in the atmosphere connected with the oceanic anomalies in the key region. Horel and Wallace (1981) noted before that, throughout the tropics, the mean tropospheric temperature varies simultaneously with sea surface temperatures in the Pacific Ocean. We find a similar result. In fact, even when the temperature is integrated over the entire mass of the Northern Hemisphere, as shown in Fig. 13b, its time series is highly correlated with the temperature record in the key region (Fig. 13a). The correlation coefficient, presented in Fig. 14, has a surprisingly high value of $r = 0.65$ for the 180-months series when the anomalies in the Northern Hemisphere temper-

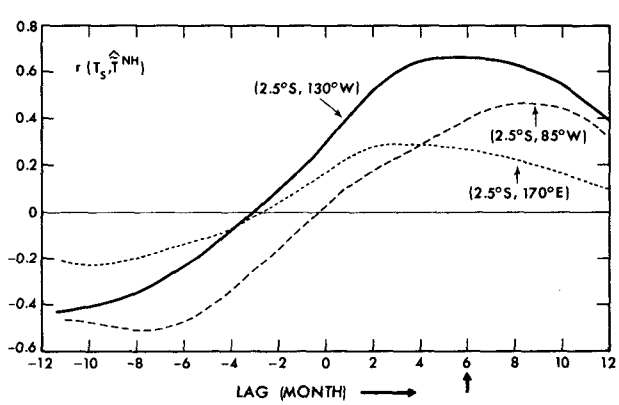

FIG. 14. Correlation coefficient between the sea surface temperature in the key region at 2.5°S, 130°W and the temperature averaged over the mass of the entire Northern Hemisphere (solid curve). Similar curves for the sea-surface temperature records off the coast of Ecuador at 85°W (dashed) and near the date line at 170°E (dotted) are shown for comparison. A positive lag indicates that anomalies in the Northern Hemisphere temperature tend to follow anomalies in the sea surface temperature.

ature lag the anomalies in the key region by 6 months. This correlation is highly significant as shown by a comparison with Table 1.

The correlation curves for all longitudes between about 100°W and 160°W are similar to the one shown for 130°W. However, as demonstrated by the dashed and dotted curves in Fig. 14 the correlations drop off considerably near the coast of South America and especially west of the date line where they are not significant at any lag. Also the correlations of the equatorial sea surface temperatures in the Atlantic and Indian Oceans with the Northern Hemispheric mean atmospheric temperatures are much weaker than those near 130°W confirming the validity of our choice of "key region." The correlation with the Southern Hemispheric temperature, although similar, is not significant perhaps because of less reliable analyses in that hemisphere. Investigating this phenomenon somewhat further we find that the main "response" takes place in the tropics in the upper troposphere. This is clear if we consider Fig. 15a which shows a cross section of the zonal mean "warm-cold" case. As suggested to the authors by Manabe (personal communication, 1982) this pattern may be due to increased moist convection in the tropics which tends to lead to the largest positive temperature changes in the upper troposphere as well as large negative changes in the lower stratosphere. The changes in the lower stratosphere may be caused by overshooting of the intensified Hadley cells into a region where dry adiabatic changes lead to cooling rather than heating (see e.g., Manabe *et al.*, 1970, their Figs. 5.8 and 5.9).

The areas in Fig. 15 where the differences are significant at or beyond the 95% level are shaded. They were computed using the same Eq. (2) as was used before in the local tests, but here applied to the zonal mean temperature and its year-to-year variance. The relative heating (cooling) of the entire tropical troposphere during warm (cold) sea surface episodes is highly significant, as is the cooling (warming) near 20°N at 50 mb. However, the changes in middle latitudes and those at high northern latitudes in the lower stratosphere are not significant at the 95% level, except for the small region near 55°N at 200 mb. The cooling near the Antarctic continent appears to be significant from our calculations. Considering the changes in humidity in Fig. 15b we find the plausible response of a substantial increase of water vapor in the lower tropical troposphere when the key region is warm versus a decrease when it is cold.

The geographic distributions for the correlations between the temperature in the key region and the 200 mb temperature field at various lags are shown in Fig. 16. This series of 4 maps illustrates well the gradual spreading of the signal from the tropical Pacific over the entire tropics, and its eventual broadening into middle latitudes going from lag = −3 to lag = +6 months. The tropical response seems to peak at a lag of about +3 months. It is of considerable interest to compare these maps with the sea-surface temperature correlation maps in Fig. 8. The two sets

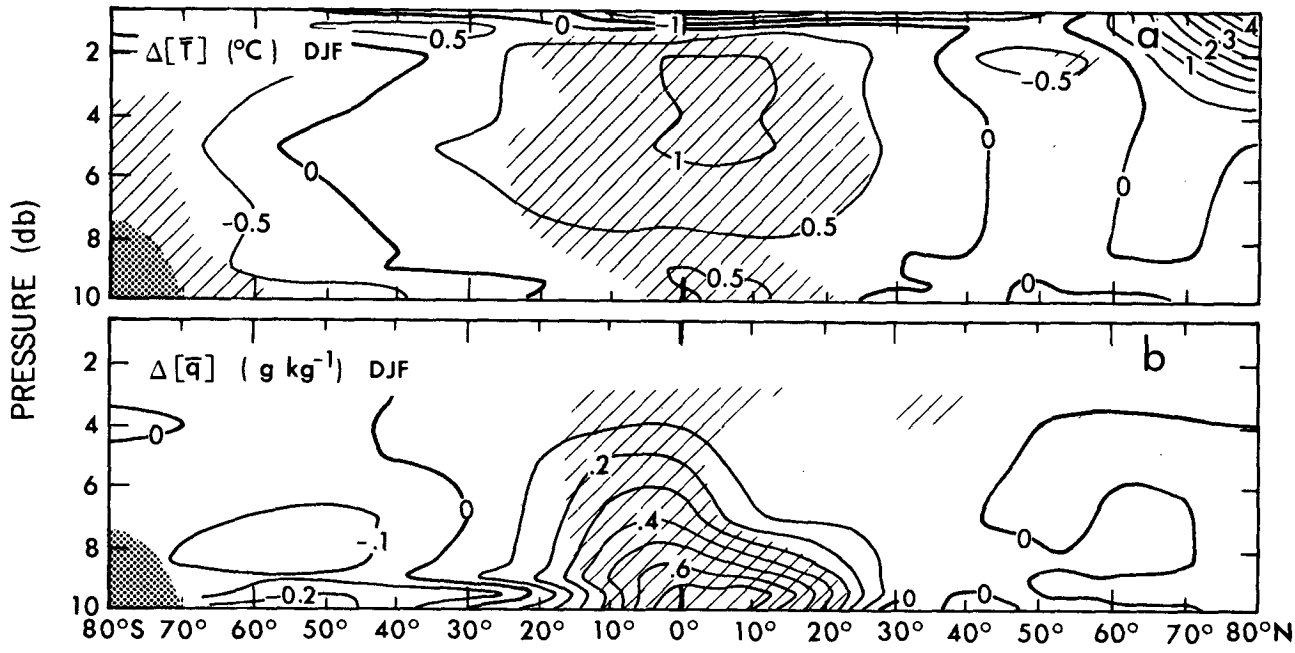

FIG. 15. Zonal-mean cross sections of (a) the average temperature difference (°C) and (b) the specific humidity difference (g kg^{-1}) between the December–February cases that $\bar{T}_s$ at 2.5°S, 130°W was relatively warm and those that it was relatively cold. The areas of significant change (≥95%) are shaded.

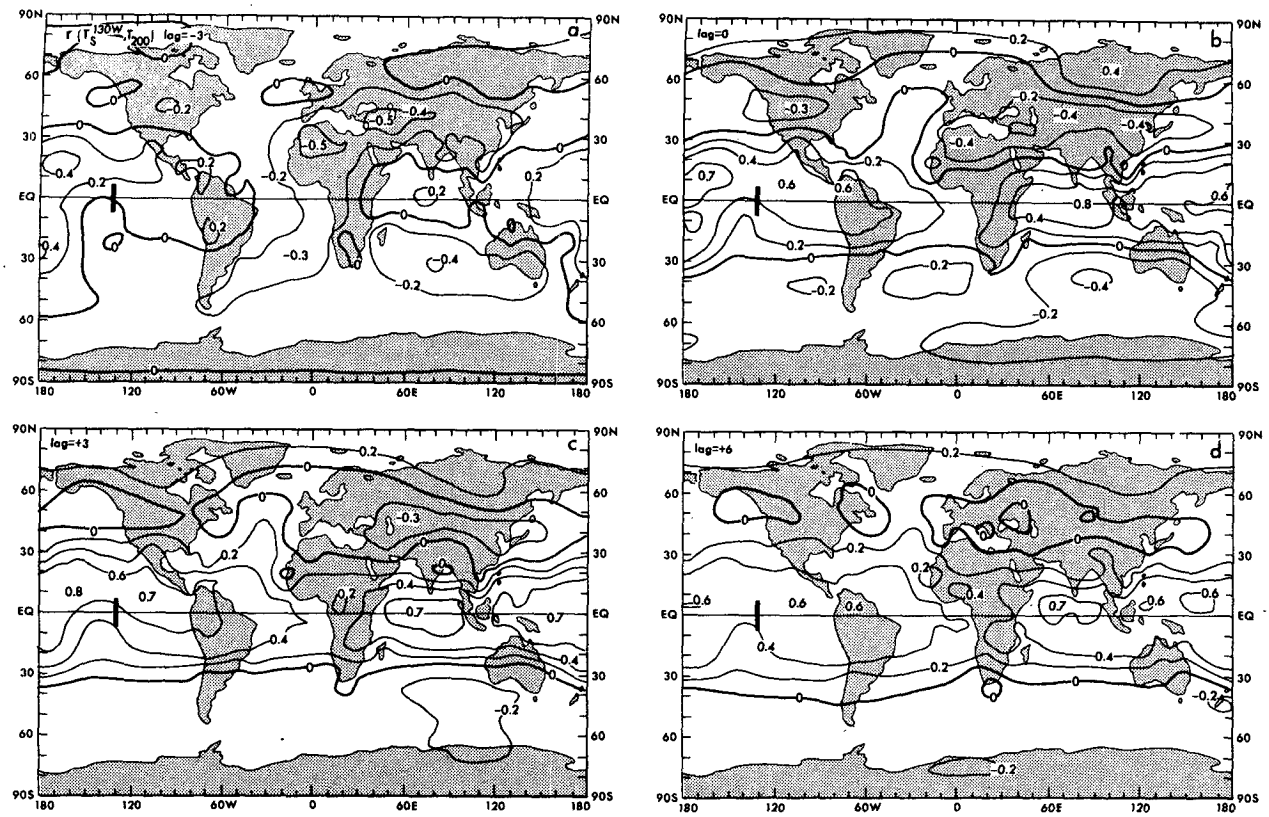

FIG. 16. Maps of the correlation coefficient of the sea surface temperature anomalies in the key region with those of the atmospheric temperature at 200 mb for various lags (in months); a positive lag indicates that the atmospheric temperature follows the one in the key region. Extensive areas with $|r| \geq 0.3$ are statistically significant at the $\geq 95\%$ level.

of maps show roughly a parallel evolution in the tropics. This similarity in evolution may explain to some extent why the atmospheric temperature response does not exhibit a maximum at lag = 0 as one might expect for convective heating, but instead 3 to 6 months later.

7. Summary and concluding comments

A key region has been identified near the equator at 130°W where large anomalies in the sea surface temperature tend to occur. These anomalies are well correlated with some of the dominant anomalies in the global atmosphere, such as those in the subtropical jets near 200 mb. The importance of the time series at 130°W longitude is probably related to the fact that it best represents the record of sea surface temperature averaged over the entire eastern tropical Pacific or, in other terms, the record of El Niño and non-El Niño episodes. As suggested by Bjerknes (1969), we find that during warm episodes the east–west Walker circulation weakens and the local north–south Hadley circulations strengthen over the eastern Pacific Ocean. The stronger Hadley cells then lead to an intensification of the subtropical jets in both hemispheres.

A rather spectacular new finding is the high correlation ($r \approx 0.6$) between the sea surface temperature record in the key region and the record of mean atmospheric temperature averaged over the mass of the entire Northern Hemisphere at a lag of +6 months. This fact suggests a possible central role of surface temperature anomalies in the equatorial Pacific in the fluctuations of the world climate during the present 15-year period.

The graphs in Fig. 17 summarize zonal-mean conditions for the warm–cold differences averaged for ten December–February and six June–August seasons in the 1963–73 record. The significance of the changes was computed from Eq. (2) using the time-mean and variance statistics of the zonal mean values for the different quantities shown. The intensification of the Hadley cells is clear with horizontal mass convergence at the surface near the equator (Fig. 17b), rising motion at 500 mb (Fig. 17g) and mass divergence at 200 mb (Fig. 17f). The curves in Fig. 17c show that ocean temperature differences are positive even when averaged over all tropical oceans. In case of the zonal wind, Fig. 17a gives rather insignificant changes near the surface, whereas Fig. 17e shows a sharp increase at the 200 mb level especially in the winter hemisphere associated with a stronger local Hadley circulation.

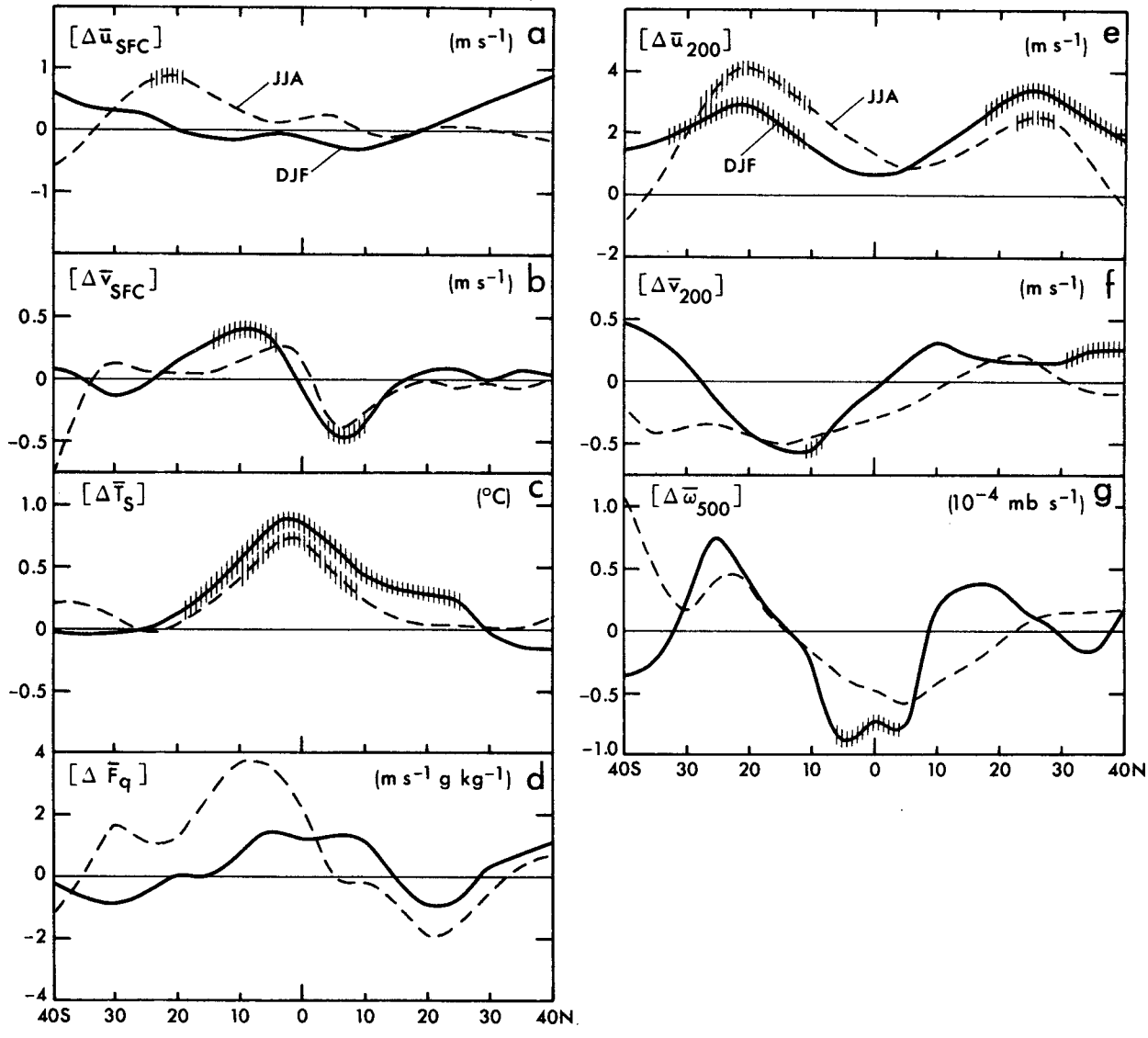

FIG. 17. Meridional profiles of (a) $[\Delta\bar{u}_{sfc}]$ in m s^{-1}, (b) $[\Delta\bar{v}_{sfc}]$ in m s^{-1}, (c) $[\Delta\bar{T}_s]$ in °C, (d) $[\Delta\bar{F}_q]$ in m s^{-1} g kg^{-1}, (e) $[\Delta\bar{u}_{200}]$ in m s^{-1}, (f) $[\Delta\bar{v}_{200}]$ in m s^{-1}, and (g) $[\Delta\bar{\omega}_{500}]$ in 10^{-4} mb s^{-1}, where the brackets indicate zonal mean values taken either over the oceans only (a–d) or over an entire latitude circle (e, f and g). The sections of the curves with significant change (≥95%) are shaded.

Let us conclude with some final comments.

1) With the aid of various statistics we have tried to diagnose a certain class of anomalies in the climate system. Thus, statistical relations, based on carefully selected observational data, were used to sketch how variations in the global atmosphere can be connected with variations in the surface temperature of the eastern equatorial Pacific Ocean. One of the important links between oceanic and atmospheric anomalies must be the anomalous surface exchange of water vapor over the key region, providing a source of latent heat for atmospheric anomalies. This exchange can be estimated from surface ship observations using the approximate relation

$$F_q = c_q\overline{|\bar{\mathbf{v}}|(q_s - q)},$$

where c_q = exchange coefficient for water vapor $\approx 1.5 \times 10^{-3}$, $\mathbf{v}$ = horizontal surface wind vector, and $q_s - q$ the difference between saturation specific humidity at sea surface temperature and the observed atmospheric specific humidity just above the surface. Based on our surface ship reports the vertical flux was computed and the resulting zonal-average difference for warm–cold episodes is presented in Fig. 17d. Although the relative increase in water vapor input into the equatorial atmosphere during warm episodes is plausible, it does not reach our 95% criterion. A value of +2 m s^{-1} g kg^{-1} on the graph is equivalent with a zonally averaged input of latent heat on the order

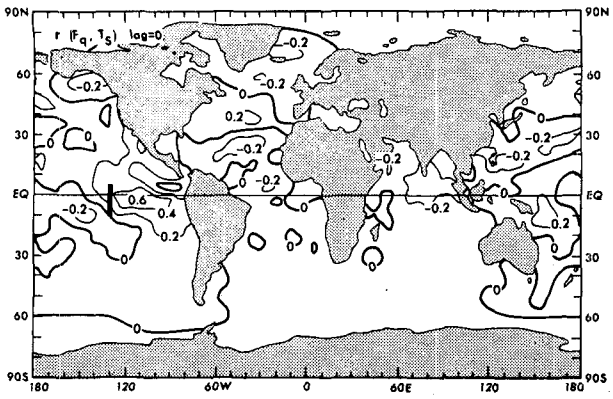

FIG. 18. Map of the correlation coefficient of the sea surface temperature in the key region at 2.5°S, 130°W with the upward flux of water vapor near the surface at lag = 0.

of 10 W m^{-2} which is not insignificant compared with the climatological annual-mean value of about 40 W m^{-2} (Oort and Vonder Haar, 1976). The corresponding correlation map in Fig. 18 shows large, positive and significant ($r \geq 0.3$) correlations over the eastern tropical Pacific where one would expect the main source of water vapor to be located.

2) In conclusion, we have isolated the sea surface temperature anomalies centered at 2.5°S, 130°W as a key index during the 1958–73 period for the pattern of climatic anomalies in the tropics and, when integrated, also for the anomalies in the global atmosphere. Of course, the findings reported here only present part of the puzzle. For example, questions on what heat source initiates and maintains the warm anomalies in the eastern equatorial Pacific Ocean and why the anomalies eventually break down are of great interest. A possible heat source may be the large reservoir of warm water normally stored in the western Pacific Ocean (Wyrtki, 1979 and 1982).

Acknowledgments. We want to thank Dr. J. Smagorinsky who provided the opportunity to pursue our joint studies at GFDL. The help of Drs. I. Orlanski and Y. Hayashi, and the critical reviews by Drs. Y. Kurihara, N.-C. Lau, S. Manabe, K. Miyakoda, G. Philander and the official reviewers are much appreciated. Special thanks are due to Mr. M. Rosenstein for help in programming, Mr. P. Tunison for drafting the figures and Ms. J. Kennedy for typing the manuscript.

REFERENCES

Arkin, P. A., 1982: The relationship between interannual variability in the 200 mb tropical wind field and the Southern Oscillation. *Mon. Wea. Rev.*, **110,** 1393–1404.

Berlage, H. P., 1966: *The Southern Oscillation and World Weather.* Commun. Trans. No. 88, Roy. Netherlands Meteor. Inst., 152 pp.

Bjerknes, J., 1969: Atmospheric teleconnections from the equatorial Pacific. *Mon. Wea. Rev.*, **97,** 163–172.

Chen, W. Y., 1982: Fluctuations in Northern Hemisphere 700 mb height field associated with the Southern Oscillation. *Mon. Wea. Rev.*, **110,** 808–823.

Chiu, W.-C., and A. Lo, 1979: A preliminary study of the possible statistical relationship between the tropical Pacific sea surface temperature and the atmospheric circulation. *Mon. Wea. Rev.*, **107,** 18–25.

Horel, J. D., and J. M. Wallace, 1981: Planetary-scale atmospheric phenomena associated with the Southern Oscillation. *Mon. Wea. Rev.*, **109,** 813–829.

Julian, P. R., and R. M. Chervin, 1978: A study of the Southern Oscillation and Walker Circulation phenomena. *Mon. Wea. Rev.*, **106,** 1433–1451.

Keshavamurty, R. N., 1982: Response of the atmosphere to sea surface temperature anomalies over the equatorial Pacific and teleconnections of the Southern Oscillation. *J. Atmos. Sci.*, **39,** 1241–1259.

Lau, K.-M. and P. H. Chan, 1983: Short-term climate variability and atmospheric teleconnection from satellite-observed outgoing long-wave radiation. Part I: Simultaneous relationships. *J. Atmos. Sci.*, **40,** (in press).

Manabe, S., J. L. Holloway, Jr. and H. M. Stone, 1970: Tropical circulation in a time-integration of a global model of the atmosphere. *J. Atmos. Sci.*, **27,** 580–613.

Namias, J., 1976: Some statistical and synoptic characteristics associated with El Niño. *J. Phys. Oceangr.*, **6,** 130–138.

Oort, A. H., 1983: *Global Atmospheric Circulation Statistics,* 1958–1973. NOAA Prof. Pap. No. 14., U.S. Government Printing Office, Washington, D.C., 180 pp.

——, and T. H. Vonder Haar, 1976: On the observed annual cycle in the ocean–atmosphere heat balance over the Northern Hemisphere. *J. Phys. Oceangr.*, **6,** 781–800.

Pan, Y.-H., 1978: The effects of the zonal circulation in the equatorial atmosphere on the relation between the surface temperature of the equatorial ocean and midlatitude westerlies. *Sci. Atmos. Sinica,* **2,** 246–252 [in Chinese]

Panofsky, H. A., and G. W. Brier, 1958: *Some Applications of Statistics to Meteorology.* The Pennsylvania State University Press, 224 pp.

Pazan, S. E., and G. Meyers, 1982: Interannual fluctuations of the tropical Pacific wind field and the Southern Oscillation. *Mon. Wea. Rev.*, **110,** 587–600.

Rasmusson, E. M., and T. H. Carpenter, 1982: Variations in tropical sea surface temperature and surface wind fields associated with the Southern Oscillation/El Niño. *Mon. Wea. Rev.*, **110,** 354–384.

Rowntree, P. R., 1972: The influence of tropical east Pacific Ocean temperatures on the atmosphere. *Quart. J. Roy. Meteor. Soc.*, **98,** 290–321.

Shukla, J., and J. M. Wallace, 1983: Numerical simulation of the atmospheric response to equatorial Pacific sea surface temperature anomalies. *J. Atmos. Sci.*, **40,** 1613–1630.

Spiegel, M. R., 1961: *Statistics.* Schaum's Outline Series in Mathematics, McGraw Hill, 359 pp.

Trenberth, K. E., and D. A. Paolino, Jr., 1981: Characteristic patterns of variability of sea level pressure in the Northern Hemisphere. *Mon. Wea. Rev.*, **109,** 1169–1189.

van Loon, H., and R. A. Madden, 1981: The Southern Oscillation. Part I: Global associations with pressure and temperature in northern winter. *Mon. Wea. Rev.*, **109,** 1150–1162.

——, and J. C. Rogers, 1981: The Southern Oscillation. Part II: Associations with changes in the middle troposphere in the northern winter. *Mon. Wea. Rev.*, **109,** 1163–1168.

Walker, G. T., and E. W. Bliss, 1932: World Weather V, *Mem. Roy. Meteor. Soc.*, **4,** 53–84.

——, and ——, 1937: World Weather VI, *Mem. Roy. Meteor. Soc.*, **4,** 119–139.

Weare, B. C., A. R. Navato and R. E. Newell, 1976: Empirical orthogonal analysis of Pacific sea surface temperatures. *J. Phys. Oceanogr.*, **6,** 673–678.

Wyrtki, K., 1979: The response of sea surface topography to the 1976 El Niño. *J. Phys. Oceanogr.*, **9,** 1223–1231.

——, 1982: The Southern Oscillation, ocean-atmosphere interaction and El Niño. *J. Mar. Tech. Soc.*, **16,** 3–10.